Integrating Materials and Manufacturing Innovation (2021) 10:299–310
https://doi.org/10.1007/s40192-021-00214-7

TECHNICAL ARTICLE

An Active Learning Approach for the Design of Doped LLZO Ceramic Garnets for Battery Applications

Juan C. Verduzco[1] · Ernesto E. Marinero[1] · Alejandro Strachan[1]

Received: 10 February 2021 / Accepted: 10 May 2021 / Published online: 26 May 2021

Abstract
Growing demand in applications like portable electronics and electric vehicles calls for cost-effective, safe, and high-performance energy storage systems. Development of solid-state electrolytes with Li^+ ionic conductivities comparable to those of the current liquid chemistries is an important step towards meeting these needs. Unfortunately, one of the most promising solid electrolytes known to date, lithium lanthanum zirconium oxide (LLZO) garnets, exhibits far from ideal ionic conductivity. Thus, significant efforts, often through aliovalent substitution, have been devoted to increasing their ionic conductivity. Given the high-dimensional design space involved and the time required for synthesis, processing, and characterization of new materials, brute force approaches are not ideal to identify optimal compositions. We assess whether machine learning tools can be used to effectively explore the design space of LLZO garnets and potentially reduce the number of experiments involved in their development. We collected, curated, and filtered all the experimental results of Li^+ ionic conductivity in LLZOs published in the scientific literature. Exploration of this data provides insights into the mechanisms that govern ionic transport in these oxides. Furthermore, we show that active learning with predictive models based on random forests can effectively be used with current data for the design of experiments. Our results indicate that the current highest Li^+ ionic conductivity garnet LLZO could have been discovered with only 30% of the experimental studies conducted to date. All data and models are available online and can be used to drive future investigations.

Keywords Active learning · Solid electrolytes · Materials design · Materials data

Introduction

The discovery, optimization, and deployment of new solid state electrolytes for energy storage with improved properties are key to future safe and high-performance batteries for portable, wearable, and transportation applications. Substitution of current liquid materials with solids would unlock an enormous potential for higher energy density and dramatically improve battery safety [1]. Solid-state electrolytes offer additional benefits in terms of operating temperature ranges, as well as increased mechanical stability and resistance to dendrite growth [2]. Unfortunately, the ionic conductivity in solid electrolytes (the highest reported value is 10^{-3} S/cm) falls short when compared to their liquid counterparts that typically exhibit values at the 10^{-2} S/cm level which are needed for commercial applications. Significant efforts are currently underway to address this gap. Current solid-state electrolyte materials can be categorized based on their chemistry; they include oxides, sulfides, hydrides, halides, and polymers. None of these materials excel in all the required properties for battery applications such as area-specific resistance, ion selectivity, chemical stability, mechanical properties, and processability [3].

Among oxides, a promising solid electrolyte is the garnet $Li_7La_3Zr_2O_{12}$ (LLZO); it shows good chemical stability against Li metal [4] and a wide electrochemical window of operation [5]. LLZO was first reported by Murugan et al. in 2007 to exhibit an ionic conductivity as high as 3.0×10^{-4} S/cm [6] at 25 °C. This garnet can crystallize in two structures, tetragonal and cubic, whose Li^+ ionic conductivity differs by two orders of magnitude at room temperature. The ionic conductivity of the garnet tetragonal phase was measured as 5.2×10^{-6} S/cm [7]. Stabilization of the cubic polymorph at room temperature via the introduction of substitutional Al atoms in the lithium

✉ Alejandro Strachan
strachan@purdue.edu

[1] School of Materials Engineering and Birck Nanotechnology Center, Purdue University, West Lafayette, IN 47907, USA

sublattice was reported with an improved ionic conductivity at 4.0×10^{-4} S/cm [8]. Ceramic garnet oxides based on LLZO have since gained popularity as the addition of aliovalent dopant elements such as Ga, Ta, Nb, and Bi results in significant improvements in the Li^+ ionic conductivity yielding values from 10^{-5} to 10^{-3} S/cm [9–11].

Based on first principles calculations, researchers have proposed a variety of substitutional elements predicted to form stable structures when added to LLZO [12], resulting in a multi-dimensional design space which remains largely unexplored both across the periodic table and compositions. Challenges in synthesis and characterization make brute force testing of a large fraction of the possible garnets impractical. Synthesis of well-consolidated garnet oxides with low porosity, critical to attaining high Li^+ conductivity, is time consuming and expensive. In addition, sintering requires high temperatures (over 1100 °C) and the garnet needs to be protected against oxidation and moisture [13]. A further hindrance in the selection of promising compositions is the lack of a complete understanding of the mechanisms underlying the effect of aliovalent dopants on Li^+ ionic conductivity. Current hypothesis is based on the interplay between the occupancy of the lithium sublattice [14–16], the changes in the lattice parameters introduced by elemental substitution [17, 18] and changes in grain growth induced by the doping elements [19, 20].

Active learning, a subset of machine learning, refers to systems that can learn dynamically by analyzing data and developing queries in an interactive process. Starting with an initial set of data points, these algorithms develop predictive models and apply them to design future data queries (experiments in our case) to test various hypotheses such as overall reduction of uncertainty or the maximization/minimization of an objective function [21]. Ling et al. [22] proposed a framework to use random forest with quantified uncertainties to guide experimental search. They found that even with relatively small datasets machine learning can be used to identify the optimal performance within in a closed pool in an optimal fashion, i.e., with the fewest experimental iterations. Our results indicate that a reduction in the number of plausible experiments by 30% is possible in efforts to synthesize garnets with high ionic conductivity. We note that this work focuses on a single figure of merit, lithium ionic conductivity, and that there are several other properties that need to be optimized on a material to have practical applications as a solid-state electrolyte.

The remainder of the paper is organized as follows. "Data Collection, Curation, Publishing, and Filtering" section discusses our data collection and curation process after which, and in "Predictive Models" section, we model the data. "Active Learning" section introduces our work on active learning and in "Conclusions" section conclusions are drawn.

Data Collection, Curation, Publishing, and Filtering

Driven by the goal of faster and less costly discovery and deployment of materials [23], significant developments in cyber-infrastructure to make materials data findable and accessible have occurred, see, for example, Refs. [24, 25]. These repositories are reliant on authors voluntarily sharing data with the community, although federal agencies often mandate data to be publicly available. Prior to our work, the data of interest for our application were not available in a minable form. Therefore, we performed an extensive literature search for Li+ experimental conductivities in ceramic materials with the garnet structure similar to LLZO. This resulted in 40 peer-reviewed publications that satisfied the following conditions: i) reported minimum values or the absence of impurity phases (in particularly Al contamination), and ii) documented procedures and values of pellet sintering temperatures, including the addition of sintering aids for pellet manufacturing. Even after this initial filtering, many of the publications lacked details of processing, microstructure, and defects known to affect lithium-ion conductivity.

The collection process resulted in information on 188 garnet oxide compositions as entries. This data collection process took approximately three months and resulted in 100 unique garnet compositions published between 2005 and 2020. Inspired by FAIR principles of making data findable, accessible, interoperable, and reusable [26], the resulting curated data were published in Citrination [27], an open platform to share datasets and models powered by Citrine Informatics. In addition, the models and tools presented here are available in nanoHUB [28], a platform for online simulations and modeling [29].

Given the high dimensionality of the data, we applied a series of additional filters to reduce the amount of experimental detail gaps. A graphical representation of these filters can be seen in Fig. 1. We focused on ionic conductivities measured between 18 and 32 °C. The density of the ceramic pellet can drastically affect ionic conductivity. Unfortunately, this parameter is often not reported in the publications collected. We used sintering temperature, a more commonly reported processing parameter, as a surrogate since high-temperature sintering often result in good compaction [30]. To account for the effect of pellet density on ionic conductivity, we included only materials processed at sintering temperatures above 900 °C. In addition, we only considered garnets stabilized into their high-ionic conductivity cubic phase and discarded those in the lower ionic conductivity tetragonal polymorph [31]. Finally, we removed duplicate data reported in different publications and replaced the ionic conductivity values with the median

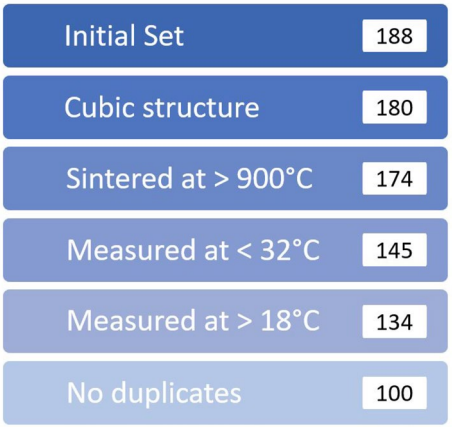

Fig. 1 Filters applied to the compositions drawn from the literature. Numbers represent how many entries were left after applying the filtering operation

of their measurements, an approach that has been reported to reduce the impact of data uncertainty [32]. In this work, we use the nominal compositions reported by the authors. We note that, due to the volatility of Li, the actual composition could deviate from these values.

The resulting data, after filtering, consists of 100 unique compositions. Each and every entry includes Li, La, and O and a combined 14 substituent elements are represented. The frequencies of the remaining elements are listed in Table 1. Similarly, Table 2 shows the frequency of the oxides of different numbers of components.

Before describing the application of data science tools for design of experiments, we explore the collected data. Li^+ ions occupy a sublattice containing (24d) tetrahedral and (96h) distorted octahedral sites in the Ia3d space group cubic garnet and the various dopants affect the occupancy of these sites. Given that ionic transport is mediated by vacancies, Fig. 2 shows the ionic conductivities of materials in our dataset as a function of Li^+ per formula unit. The colors indicate distinct main dopant, i.e., the element with the larger atomic ratio between the dopant and the element in the site occupied. It is clear from the plot that the chemical nature of the dopant is important. In addition, it is also evident that a rough maximum in conductivity exists around 6.3–6.5 Li^+ per formula unit, representing a sublattice occupancy of 50–52 out of the 72 possible sites. The number of available sites is given by 24+96/2 as octahedral sites occur in neighboring pairs that cannot be simultaneously occupied be two ions [14].

This maximum Li-site occupancy likely indicates an optimal balance between Li^+ and vacancy concentrations and agrees with prior compilations of LLZO-based ceramic garnets [33]. We note that Thompson et al. [34] observed a maximum in conductivity in Ta-doped garnets near 6.5 Li^+ per formula unit and attributed the decrease after the maximum to a transformation from the cubic to the tetragonal phase. In our case, all data points correspond to the cubic phase.

Table 1 Frequency per substituent element

Element	Frequency	Element	Frequency
Zr	70	Gd	10
Nb	40	Ca	7
Ta	29	Bi	6
Ga	16	Al	5
Y	15	Sc	3
Sr	11	Nd	3
Ba	10	Sb	2

Predictive Models

Machine learning tools, specifically active learning, have been shown capable of reducing the number of experiments required to achieve a design goal, see, for example, Refs. [35, 36]. The predictive accuracy of the underlying models and, consequently, the efficacy of the approach, relies heavily both on the amount of training data and on the choice of descriptors or features used to express each entry [37]. Good descriptors uniquely describe the materials involved, should be significantly less onerous than the model output property, and are expected to correlate with the quantity of interest. This presents an opportunity to incorporate domain knowledge and physical intuition into otherwise agnostic models [38].

We found that the *Materials-Agnostic Platform for Informatics and Exploration* (Magpie) descriptors from Matminer [39] provides an appropriate set of descriptors for our application. Magpie includes information that can be easily obtained from composition such as valence orbital information, elemental fractions, and ionic properties. All descriptors that showed no variability across our database were removed.

Groups of descriptors are listed in Table 3. Elemental properties consist of statistical values (mean, mode, and maximum) of properties of the elements involved. Elemental fractions represent the atomic fraction of each element

Table 2 Frequency per number of components in garnet oxide

Num. components	Frequency
4 Component Oxides	6
5 Component Oxides	62
6 Component Oxides	31
7 Component Oxides	1

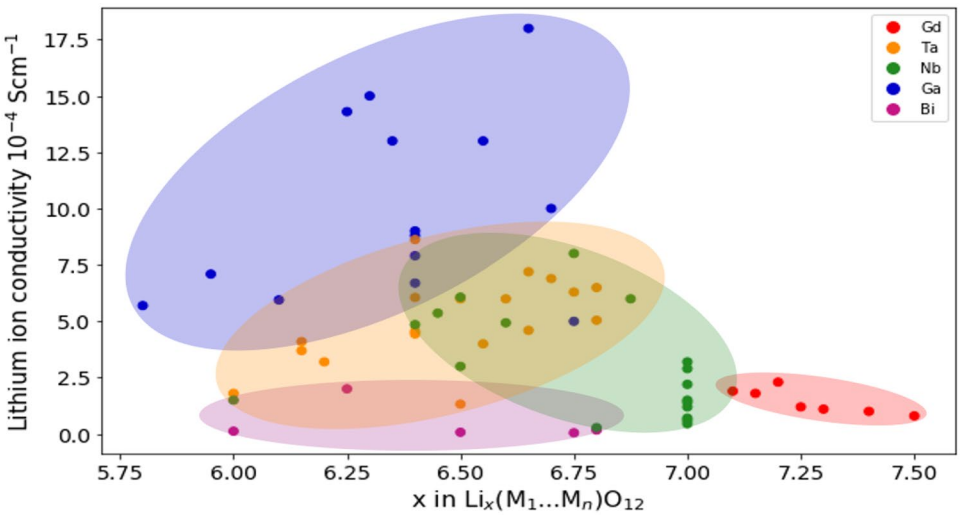

Fig. 2 Distribution of ionic conductivity against Li^+ per formula unit. Shaded areas group values for the different aliovalent dopants represented in the literature

Table 3 Descriptors used to characterize materials by their compositions. Subsets of descriptors are obtained from the magpie platform and melting temperature is taken from the original publication of the data point

Attributes	Number of attributes
Elemental properties	77
Elemental fractions	17
Stoichiometric attributes	6
Valance orbitals	4
Experimental temperature	1

contained in the composition. Stoichiometric attributes represent the fraction of elements present in the composition and several L^p norms of these fractions. These attributes are independent of the elements involved. Valence orbitals represent the average fraction of electrons in each of the valence shells between elements present. Finally, the temperature of the experimental measurement of the ionic conductivity was added as an additional descriptor, resulting in a total of 105.

As referenced above, lithium ionic conductivity in cubic LLZO-type garnets has been shown to have a maximum for lithium per formula unit near to 6.3–6.5 Li^+, a phenomenon discussed in "Data Collection, Curation, Publishing, and Filtering" section. This quantity is fed to the model via descriptors like the elemental fractions and stoichiometric attributes. For example, elemental fractions take values of the atomic fraction related to whether any element from the periodic table is present in the composition. Thus, this descriptor effectively captures the distribution shown in Fig. 2.

After identifying the data and descriptors, we explore two widely used machine learning tools for regression, random forests (RFs), and artificial neural networks (ANNs). RF models consist of an ensemble of decision trees, structures that perform tests to discriminate entries based on its attributes. For regression, the model returns an average prediction from the outputs of each tree, to limit the drawbacks in performance from decision trees when working with nonlinear data. RF models were created to counter the tendency of individual decision trees to overfit. ANNs are biologically inspired, universal approximators of nonlinear convex functions. They have been successfully used in materials science, chemistry and many other physical sciences, see for example [40–42]. It is important to recognize that small datasets represent a challenge for machine learning models, in particular ANNs [43], and thus, the predictive results need to be developed and used with this in mind.

Significant progress has been made in uncertainty quantification for RFs, and this has been implemented in the random forests with Uncertainty Estimates for Learning Sequentially (FUELS) framework described by Ling et al. [22]. Here a sample-wise uncertainty estimate can be obtained by evaluating the average of the infinitesimal jackknife variance and the jackknife-after-bootstrap variance [44] estimates plus a Monte Carlo sampling correction term. Calibration of the uncertainty when compared to the error of the prediction can be gauged by the calculation of residuals, normalized by the sample uncertainty, as perfectly calculated uncertainties would be represented by a Gaussian distribution with zero mean and unit standard deviation.

For our model RFs, the number of estimators (trees) was optimized up to a point in which no further improvement was observed and set at 500 estimators. Trees were allowed unrestricted depth to encourage them to grow until no more divisions are possible. Data were not normalized for the random forest. The dataset was split into 90% training and 10% testing. No independent validation set is used, as RFs models with bootstrap aggregation take into account the error of trained trees on a subset of the training data unseen by these estimators, the basis for the out-of-bag error. Models and uncertainty estimates implemented in this study were

implemented using tools from the open source Lolo scala library [45].

In the case of ANNs, we created an architecture with three densely connected hidden layers in a feed-forward network. The optimizer used was Adam, an adaptive learning rate algorithm [46]. Loss observed was mean absolute error (MAE). We used RELU (REctified Linear Unit) activation functions. All bias terms were initialized to zero, and all weights were initialized from random values sampled from a normal distribution of mean zero and unit standard deviation. A 20% Dropout regularization was added between each of the layers. Models with other regularization techniques and varying architectures result in similar, if slightly worse, accuracy; those results can be found in the online tool [28]. The data were split into 90% training and 10% testing sets. From the training subset, 10% was sequestered from the backpropagation and used as a stopping criterion. The optimization stops once the MAE on this sub-set fails to decrease by at least 1×10^{-10} for 1000 steps to limit overfitting. Data were normalized using a standard score normalization. The network was trained with an early stopping criteria [47] to avoid overfitting by restoring the parameters to those of the best epoch in terms of the validation set MAE. Implementation of this network was through the Tensorflow/Keras software package [48].

Figure 3 showcases the performance of these algorithms as a parity plot comparing experimental values of lithium ionic conductivity with model predictions. Green dots represent training data and red denotes testing. Repeating the training ten times with random selection of training and testing data results in an average MAE on the testing set of 1.09×10^{-4} S/cm for the ANN and 0.92×10^{-4} S/cm for the RF. While neural networks often outperform random forests for regression predictions for different materials properties [49], we find comparable performance for our dataset in the average testing MAE. Having established similar accuracies and given the significant work on uncertainty quantification on RFs (important for active learning) we will continue this study with RFs and framework for uncertainty estimates proposed by Ling et al. [22].

Visual inspection of Fig. 3 indicates that the RFs are able to assign larger uncertainties to cases where the predicted mean deviates the most from the experimental values. To assess the accuracy of the uncertainty estimates of the RFs, we computed the distribution of residuals of the mean prediction of the RFs normalized by their uncertainty through a 10-fold cross-validation, see Fig. 4. Accurate models and uncertainty estimates would result in a Gaussian distribution with mean of zero and unit standard deviation. We find a small left skew (residuals are defined as the model prediction minus the true experimental value), indicating a tendency of the model to slightly overpredict the properties. We attribute this overestimation of ionic conductivities by the RFs to the high dimensionality of compositional space and sparse training data. As can be seen in Table 1, representation of dopants is uneven and the testing set might contain elements that are not represented in the training, like Sc, Nd, and Sb. Elements might

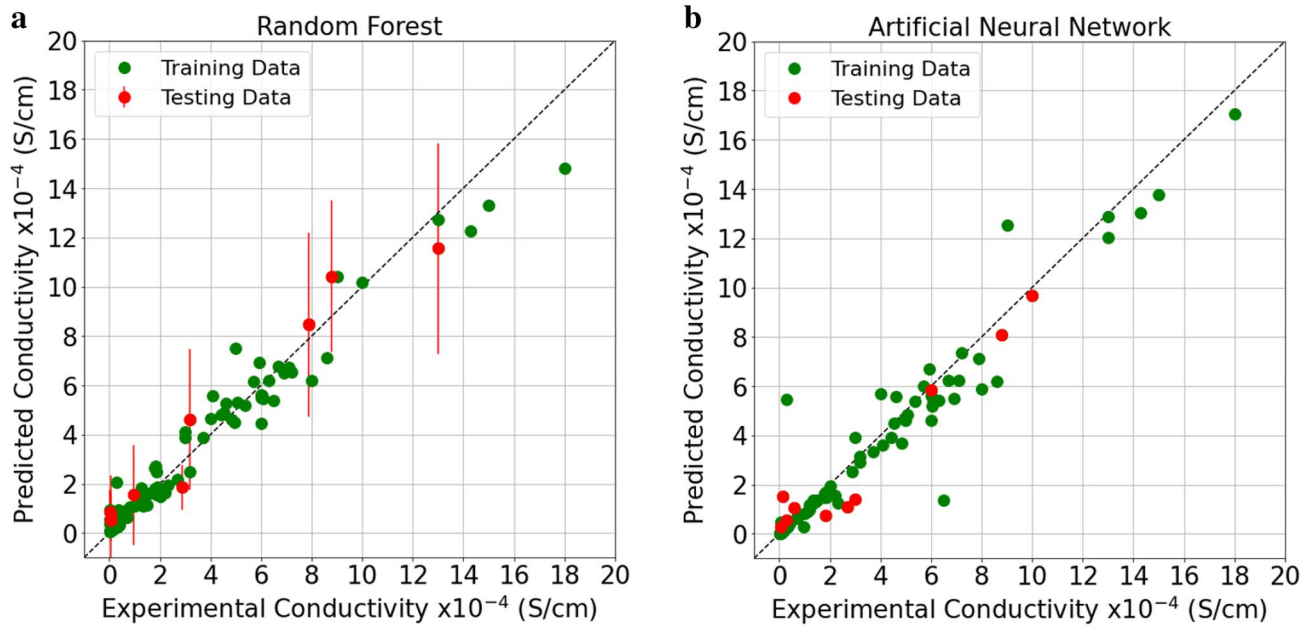

Fig. 3 Parity plots for prediction of Li-ion conductivity in garnets using **a** random forest with uncertainty and **b** artificial neural network. The training set for the models is shown in green, while the testing set is shown in red. Uncertainty estimates are included for the random forest

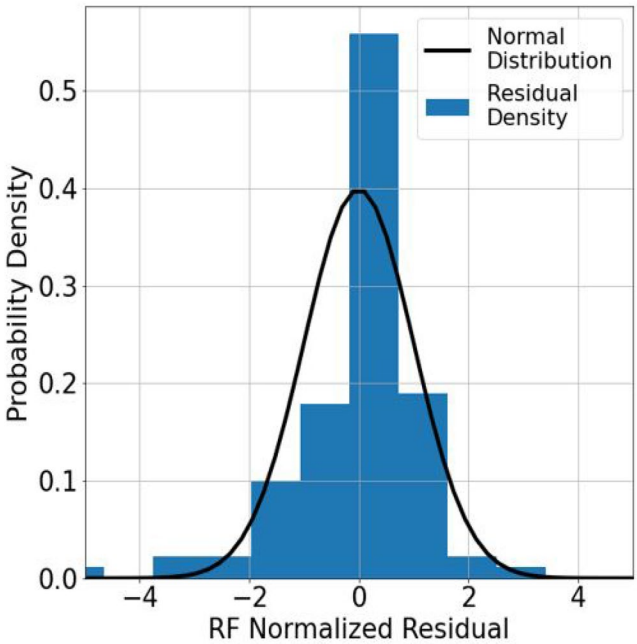

Fig. 4 Probability densities of normalized residuals computed via tenfold cross-validation for the random forest. Solid line represents perfectly calibrated uncertainties

also be present in the available data only as part of co-doped substitutions, an interplay that is only addressed in the generation of the descriptors. Also, we note the uncertainty in the data itself affects the model performance, as the measured values for conductivity can be affected by the experimental setups for synthesis and the measurement techniques. Something that is relatively unique to this problem deals with the density of the ceramic pellets, which is sometimes not reported in the literature but can drastically affect the ionic conductivity measurements for the same composition [30].

To better understand the performance of the models, we now analyze a selected test set in detail. Table 4 lists the compositions in the test set (that the model has not seen) in increasing order of experimental ionic conductivity and includes experimental values, mean RF predictions, discrepancies, and RF uncertainty estimate. This set corresponds to the set shown in Fig. 3a.

Importantly, this model can accurately rank these compositions, capturing the trends seen for different dopants. These predictions are in remarkable agreement with the experimental values considering the limited data obtained from the literature and the selection of descriptors based solely on the material composition. In this example, deviations of some of the predictions can be attributed to the materials containing one or more of the infrequent elements listed in Table 1: Ca, Sc, Bi, Al, and Sb. The model had only limited information during training on how these specific dopants affect conductivity. Regarding uncertainties, it is also interesting to note that an increase in the predicted mean values results in larger uncertainties, which would indicate that the model understands that it needs to estimate greater uncertainties for these points. In order to address the challenge posed by the

Table 4 Compositions included in the testing set of our random forest model

Composition	Experimental ionic conductivity 10^{-4} S/cm	RF prediction 10^{-4} S/cm	Residual	RF uncertainty
$Li_6La_2Nb_2Ca_1O_{12}$	0.016	0.844	0.828	0.883
$Li_6La_2Nb_2Sr_1O_{12}$	0.042	0.545	0.503	0.712
$Li_{6.75}La_3Zr_{1.75}Bi_{0.25}O_{12}$	0.05	0.704	0.654	1.226
$Li_6La_2Sb_2Sr_1O_{12}$	0.066	0.703	0.637	0.896
$Li_5La_3Nb_{1.75}Y_{0.25}O_{11.95}$	0.968	1.545	0.577	2.016
$Li_7La_{2.5}Zr_{1.5}Nb_{0.5}Ca_{0.5}O_{12}$	2.9	1.799	−1.101	0.946
$Li_{6.2}La_3Zr_{1.2}Ta_{0.8}O_{12}$	3.2	4.771	1.571	2.802
$Li_{6.4}La_3Zr_2Ga_{0.1}Al_{0.1}O_{12}$	7.9	8.364	0.464	3.517
$Li_{6.4}La_3Zr_2Ga_{0.15}Al_{0.05}O_{12}$	8.8	10.158	1.358	2.868
$Li_{6.35}La_3Zr_2Ga_{0.25}Sr_{0.1}O_{12}$	13	11.443	−1.557	4.209

three orders of magnitude variation in experimental ionic conductivities, we also trained a model on the logarithm of the ionic conductivity but found no improvements in the testing MAE. Details on the transformations of the target ionic conductivity data are detailed in Figure 1 of the Supplementary Material.

To further explore the model, we characterized the predictions as a function of Ta content, since multiple data points exist. For this analysis, we will use the model described in "Predictive Models" section and used for Fig. 3a and Table 4, keeping the same training and testing data. We explore how the model would predict for one of the most common elements in the database, Ta. We explore the model's interpolation between experimental values and its accuracy for Ta doping in Fig. 5. We plot the predicted ionic conductivities for $Li_{7-x}La_3Zr_{2-x}Ta_xO_{12}$ garnets as a function of x and include the experimental results (individual experimental are shown as open circles and the median values used for training or testing are shown as crosses). Since RFs are mathematically incapable of extrapolation, we select the range so that the predictions were not outside of the bounds of the training data. We find that the model is able to capture the overall trends of how the addition of Ta affects ionic conductivity. Differences in the literature reported values speaks to the significant effect of experimental conditions, in particular on sintering temperatures and densities, and can help explain some of the uncertainties and discrepancies in the model.

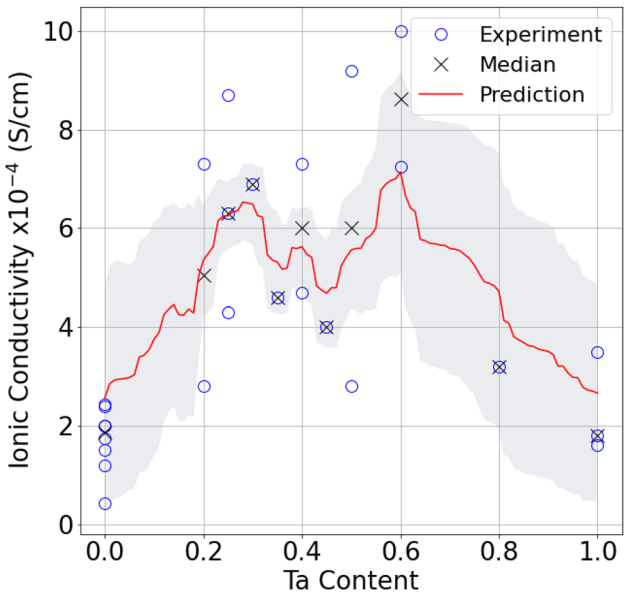

Fig. 5 Ionic conductivity of Ta-doped LLZO as a function of composition. Experiments are marked with open circles. Median of duplicate experiments are marked with crosses. RF predictions are marked with a red line with their corresponding uncertainties

Having established the ability of the RF model to describe the experimental data, we illustrate its ability to generalize and explore the space spanned by a pair of dopants. To generate this test space, we use a grid of compositions with the selected pair of dopants and establish the overall composition following the nominal stoichiometric rules to ensure stable structures. For example, following Wagner et al. [50] we consider that a Bi (5+) replaces one Zr (4+) atom and one Li(+) atom to create compositions following $Li_{7-x}La_3Zr_{2-x}Bi_xO_{12}$. Figure 6 shows color-intensity plots of the predicted ionic conductivity, for three different pairs of dopants. Experimental compositions in our dataset are marked as diamonds, and compositions that were part of the testing set are marked with an extra cross. All mapped compositions have measured temperature input at 25 °C. Figure 6 clearly shows constant value bands since the RFs models would output constant values outside of their training range.

These maps can help understand how and what the model learned from its training, even though most of the compositions do not have experimental values to validate our predictions. Figure 6a maps space including significant experimental data while Fig. 6b shows a case where the two dopants have been explored individually but not in combination. Finally, Fig. 6c explores the dopants of the best performers experimentally reported (Ga, Sc). The plots reveal how the RFs divide space and generalize from the training data. These models are tools for interpolation in a high dimensional space, thus results that involve extrapolation should be used with extreme precaution. These models, both RFs and ANNs, are available for online, interactive, simulations in nanoHUB as a Jupyter notebook "Machine learning guided design of ceramic oxides for batteries", accessible through a tool [28] in which users can access and run the models or retrain them changing hyperparameters within the online tool.

Active Learning

Following our general analysis on the performance of the models, we now focus on active learning. For this endeavor, we will posit an artificial problem where we start with 10 data points out of the 100 total and try to find the highest conductivity garnet in the fewest number of experiments. At each step of the active learning workflow, we train a RF with the available data and use it to select one of the hidden experiments to be revealed next; in a real application this would involve running an actual experiment. The selection of the most promising new experiment is done using various information acquisition functions, discussed below. We follow the framework proposed by Ling et al. [22].

We compare four information acquisition functions: maximum likelihood of improvement (MLI), upper

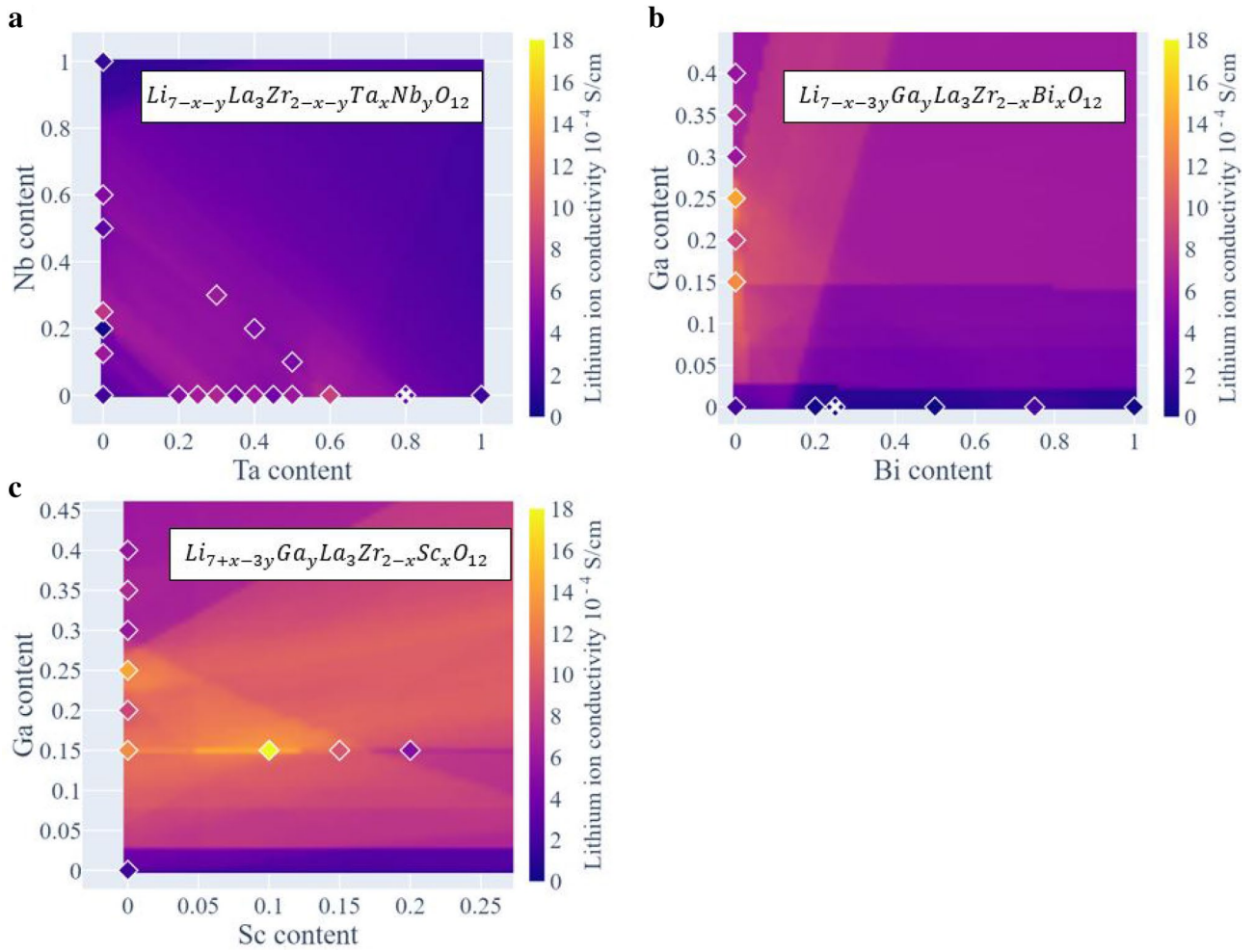

Fig. 6 Random forest model predictions for a grid of possible combinations in a dual-dopant space. Diamonds represent experimental data from the training

confidence bound (UCB), maximum expected improvement (MEI), and maximum uncertainty (MU) against a random benchmark. To determine the next candidate to query, each of these functions will explore the compositional space according to their respective equations.

- MLI tells us that we are expecting to query a region for which we see an improvement and sufficient uncertainty to have a high likelihood of getting a larger value.

$$x^* = \arg\max \frac{E[M(x_i)] - E[M(x_{\text{best}})]}{\sigma[M(x_i)]}$$

- UCB queries the sample with the maximum value of its mean prediction plus its uncertainty.

$$x^* = \arg\max[E[M(x_i)] + \sigma[M(x_i)]]$$

- MEI takes the maximum value of the prediction of the model over the possible experiments to run.

$$x^* = \arg\max E[M(x_i)]$$

- MU queries the sample with the highest uncertainty, regardless of the expected mean value.

$$x^* = \arg\max \sigma[M(x_i)]$$

In these equations, x^* represents the next sample to query, x_i are the possible experiments to run, x_{best} is the current best result in our training set, and $E[M(x)]$ is the expected value of the prediction of the model at point x. The "arg max" (arguments of the maxima) operation returns the sample where the function is maximized.

Our exercise starts with 10 randomly selected entries out the 100 total and iteratively applies active learning until the highest ionic conductivity is found. At each step, we use

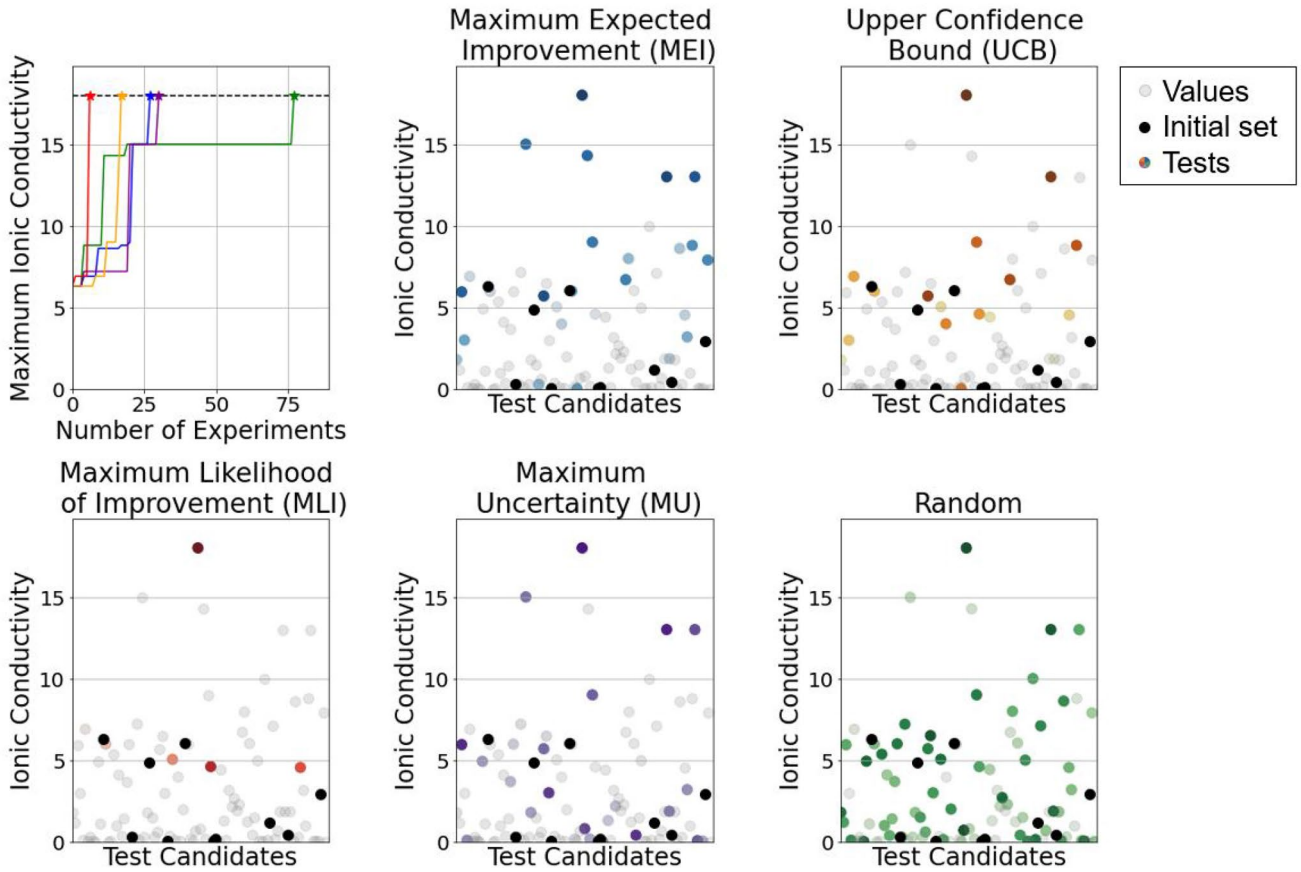

Fig. 7 Comparison of different information acquisition functions. Black dots indicate the starting initial set. Gray dots represent unknown but available points for queries. Colored dots indicate the points explored by the active learning approach. The first plot is a summary in which we track the highest value of ionic conductivity queried by the functions against the number of experiments. An animated version of the exploration is available on nanoHUB.org [28]

the available data to develop a model and use the model in conjunction with the each of the information acquisition functions to select the next experiment from the list of hidden entries. If the chosen entry is not the maximum, it will be added to the set and the cycle starts again. Figure 7 presents the results of the various acquisition functions and a benchmark of random selection. Black dots indicate the initial set that is common to all acquisition functions, gray points show the values that are unknown to the model but are available for querying, the colored points indicate values that were explored by each of the acquisition functions prior to reaching the maximum value from our closed pool, light to dark indicate selection order. The first panel shows a trendline that keeps track of the best conductivity for individual acquisition as a function of active learning step.

It is clear that all acquisition functions outperform random sampling. MEI, UCB, and MLI can find the optimal candidate in about 30% of the attempts required by random sampling and far below the cost for a brute force approach to run the entire closed pool of simulations. These three information acquisition functions take an exploitative approach to explore the space, as they use values that are similar to the maximum value that has already been found and trained on. UCB and MLI also make use of information about model prediction uncertainty. As a result, they explore compositions that have relatively high predictions for conductivity while keeping low values unexplored. In contrast to these exploitative functions, MU is an approach for exploration, which compares well against random in this application, but does not guarantee maximizing a conductivity value as it depends primarily on the uncertainty regions.

To quantify the relative performance of each information acquisition function, we performed this experiment 30 times with a randomly chosen set of 10 points for the initial set. The results, Fig. 8a, show that active learning can reduce the number of experiments required to reach the best candidate to less than 50% of the runs when compared to randomly sampling out of the remaining points in our closed pool. We note that this is an estimate and the set of possible experiments come from the literature and were chosen by experts.

To further evaluate the potential reduction of the design time, we conducted a test in which we started with an initial

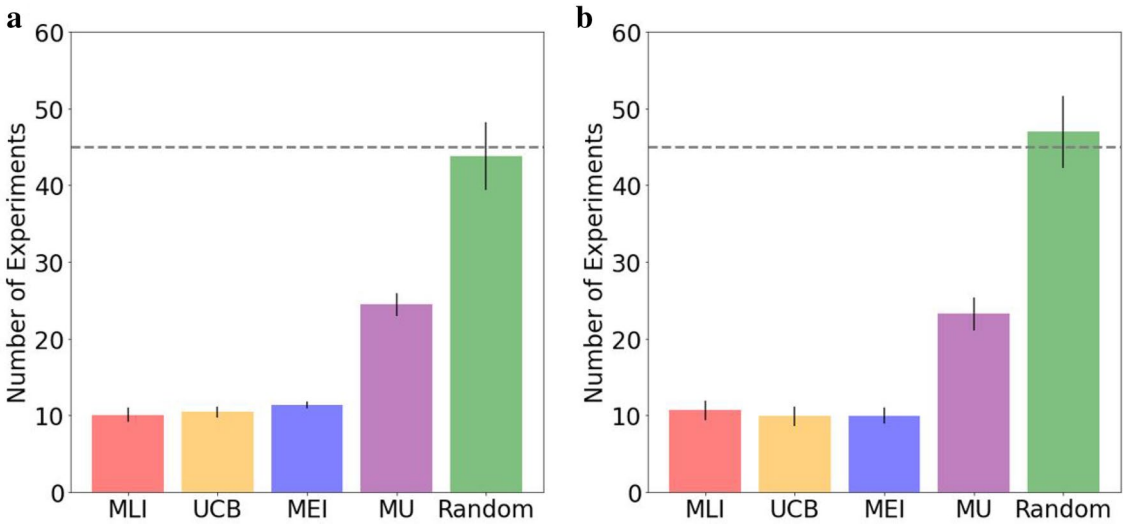

Fig. 8 Mean number of predictions per information acquisition functions for the 30-trial runs of the active learning model. Dashed line represents half of the experiments. In a the model samples 10 experiments at random. In b the model starts with the 10 oldest experiments. Black lines represent the sample standard error $E(x) = \frac{\sigma}{\sqrt{30}}$. Colors are matched to Fig. 7 for visual comparisons

set containing the 10 earliest experiments in our dataset. These compositions are listed in Table 1 of the Supplementary material and include LLZO, first reported in 2007 [6]. The results of this study are shown in Fig. 8b.

The convergence criterion for our demonstration is finding the material with the highest ionic conductivity. In a real-world application this will be determined by achieving a desired value or spending an experimental budget. To drive this point, we speculate what the timeline of published results on LLZO-type garnets would have looked like if the experimental work had been informed by the random forest framework. In Fig. 9, we start from the 10 oldest experiments and we allow the acquisition function to select which material to synthesize next. Each subsequent point sits at a spot marked by the publication of a new material.

Conclusions

We used data collection, curation, filtering, and modeling to explore the applicability of materials informatics approaches in the context of Li+ ion conductivity in doped garnets. We generated a cost-efficient set of descriptors based on published literature and domain knowledge of the problem at

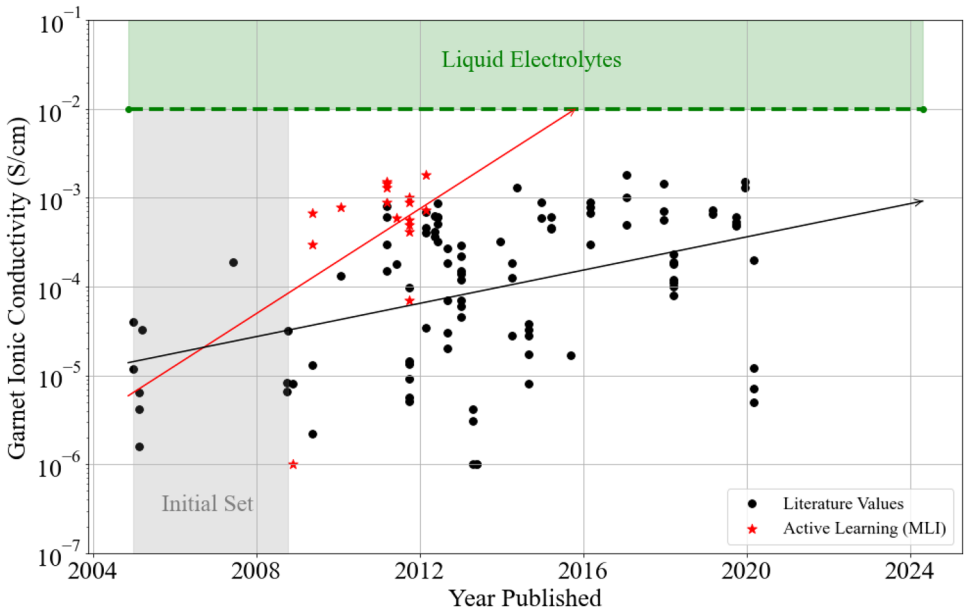

Fig. 9 Possible timeline of published experiments informed with the maximum likelihood of improvement acquisition function. Each point represents one material and when it was published. Black points represent when literature values were published. Red points indicate points explored by the function before finding the optimal candidate

hand that allowed us train models for the high-dimensional compositional space starting with a limited dataset of records from the literature. We created and compared ANNs and RFs and evaluated their performance to predict ionic conductivity from composition. We took special interest in the various sources of error in this process of using machine learning for material science, including discrepancies in the reported literature data and differences in how much each particular element is represented.

Building on these models, we assessed the possible use of active learning on experiments selection. We compared different acquisition functions within the active learning framework to assess how many tries it would be needed starting from a small subset of the data to find our best performer. We found that the best performer can be found using only 50% of the experiments that a random sampling of our unknowns would require. In addition, we evaluated how many experiments would it take if we started with the oldest points in the initial dataset to find the optimal candidate found to date, and found that we still show a 30% reduction in the number of experiments needed. Our results show that active learning approaches like the one described here can contribute to design of experiments.

In general, active learning approaches are restricted by the size and underlying dimensionality of the initial dataset for the application, the creation of an accurate surrogate model and the constraints of querying results from the information sources. Our results mirror other successful studies that made use of active learning to guide experimental searches for materials discovery with limited datasets [51, 52].

Supplementary Information The online version contains supplementary material available at https://doi.org/10.1007/s40192-021-00214-7.

Acknowledgements This effort was supported by the US National Science Foundation, DMREF program, under Contract Number 1922316-DMR. We acknowledge computational resources from nanoHUB and Purdue University through the Network for Computational Nanotechnology. J. C. V. thanks the Mexican Consejo Nacional de Ciencia y Tecnolog-a, CONACYT, for partial financial support of this research.

Compliance with ethical standards

Conflict of interest On behalf of all authors, the corresponding author states that there is no conflict of interest.

References

1. Varzi A, Raccichini R, Passerini S, Scrosati B (2016) Challenges and prospects of the role of solid electrolytes in the revitalization of lithium metal batteries. J Mater Chem A 4(44):17251–17259
2. Agrawal RC, Pandey GP (2008) Solid polymer electrolytes: materials designing and all-solid-state battery applications: an overview. J Phys D Appl Phys 41(22):223001
3. Manthiram A, Xingwen Yu, Wang S (2017) Lithium battery chemistries enabled by solid-state electrolytes. Nat Rev Mater 2(4):1–16
4. Kumazaki S, Iriyama Y, Kim K-H, Murugan R, Tanabe K, Yamamoto K, Hirayama T, Ogumi Z (2011) High lithium ion conductive $Li_7La_3Zr_2O_{12}$ by inclusion of both Al and Si. Electrochem Commun 13(5):509–512
5. Thompson T, Yu S, Williams L, Schmidt RD, Garcia-Mendez R, Wolfenstine J, Allen JL, Kioupakis E, Siegel DJ, Sakamoto J (2017) Electrochemical window of the Li-ion solid electrolyte $Li_7La_3Zr_2O_{12}$. ACS Energy Lett 2(2):462–468
6. Murugan R, Thangadurai V, Weppner W (2007) Fast lithium ion conduction in garnet-type li7la3zr2o12. Angew Chem Int Ed 46(41):7778–7781
7. Il'ina EA, Andreev OL, Antonov BD, Batalov NN (2012) Morphology and transport properties of the solid electrolyte $Li_7La_3Zr_2O_{12}$ prepared by the solid-state and citrate-nitrate methods. J Power Sources 201:169–173
8. Rangasamy E, Wolfenstine J, Sakamoto J (2012) The role of Al and Li concentration on the formation of cubic garnet solid electrolyte of nominal composition $Li_7La_3Zr_2O_{12}$. Solid State Ion 206:28–32
9. Buannic L, Orayech B, Del Amo J-ML, Carrasco J, Katcho NA, Aguesse F, Manalastas W, Zhang W, Kilner J, Llordes A (2017) Dual substitution strategy to enhance Li+ ionic conductivity in $Li_7La_3Zr_2O_{12}$ solid electrolyte. Chem Mater 29(4):1769–1778
10. Mori D, Sugimoto K, Matsuda Y, Ohmori K, Katsumata T, Taminato S, Takeda Y, Yamamoto O, Imanishi N (2019) Synthesis, structure and ionic conductivity of garnet like lithium ion conductor $Li_{6.25+x}Ga_{0.25}La_{3-x}Sr_xZr_2O_{12}$. J Electrochem. Soc. 166(3):A5168–A5173
11. Tong X, Thangadurai V, Wachsman ED (2015) Highly conductive li garnets by a multielement doping strategy. Inorg Chem 54(7):3600–3607
12. Miara LJ, Richards WD, Wang YE, Ceder G (2015) First-principles studies on cation dopants and electrolyte| cathode interphases for lithium garnets. Chem Mater 27(11):4040–4047
13. Li Y, Wang Z, Li C, Cao Y, Guo X (2014) Densification and ionic-conduction improvement of lithium garnet solid electrolytes by flowing oxygen sintering. J Power sources 248:642–646
14. Meier K, Laino T, Curioni A (2014) Solid-state electrolytes: revealing the mechanisms of li-ion conduction in tetragonal and cubic llzo by first-principles calculations. J Phys Chem C 118(13):6668–6679
15. Kihira Y, Ohta S, Imagawa H, Asaoka T (2013) Effect of simultaneous substitution of alkali earth metals and Nb in $Li_7La_3Zr_2O_{12}$ on lithium-ion conductivity. ECS Electrochem Lett 2(7):A56–A59
16. Jalem R, Rushton MJD, Manalastas W Jr, Nakayama M, Kasuga T, Kilner JA, Grimes RW (2015) Effects of gallium doping in garnet-type $Li_7La_3Zr_2O_{12}$ solid electrolytes. Chem Mater 27(8):2821–2831
17. Wang Y, Richards WD, Ong SP, Miara LJ, Kim JC, Mo Y, Ceder G (2015) Design principles for solid-state lithium superionic conductors. Nat Mater 14(10):1026–1031
18. Zhang Y, Chen F, Li J, Zhang L, Jiajun G, Zhang D, Saito K, Guo Q, Luo P, Dong S (2018) Regulation mechanism of bottleneck size on Li+ migration activation energy in garnet-type $Li_7La_3Zr_2O_{12}$. Electrochim Acta 261:137–142
19. Su J, Huang X, Song Z, Xiu T, Badding ME, Jin J, Wen Z (2019) Overcoming the abnormal grain growth in ga-doped $Li_7La_3Zr_2O_{12}$ to enhance the electrochemical stability against li metal. Ceram Int 45(12):14991–14996
20. Schwanz DK, Villa A, Balasubramanian M, Helfrecht B, Marinero EE (2020) Bi aliovalent substitution in $Li_7La_3Zr_2O_{12}$ garnets: Structural and ionic conductivity effects. AIP Adv 10(3):035204

21. Settles B (2011) Synthesis lectures on artificial intelligence and machine learning: active learning. Morgan & Claypool Publishers, San Rafael
22. Ling J, Hutchinson M, Antono E, Paradiso S, Meredig B (2017) High-dimensional materials and process optimization using data-driven experimental design with well-calibrated uncertainty estimates. Integr Mater Manuf Innov 6(3):207–217
23. National Science and Technology Council (US) (2011) Materials genome initiative for global competitiveness. Executive Office of the President, National Science and Technology Council
24. Jain A, Ong SP, Hautier G, Chen W, Richards WD, Dacek S, Cholia S, Gunter D, Skinner D, Ceder G, Persson KA (2013) The materials project: a materials genome approach to accelerating materials innovation. APL Mater 1(1):011002
25. O'Mara J, Meredig B, Michel K (2016) Materials data infrastructure: a case study of the citrination platform to examine data import, storage, and access. JOM 68(8):2031–2034
26. Wilkinson MD, Dumontier M, Aalbersberg IJJ, Appleton G, Axton M, Baak A, Blomberg N, Boiten J-W, Santos LBS, Bourne PE et al (2016) The fair guiding principles for scientific data management and stewardship. Sci Data 3:160018
27. Verduzco JC (2019) Database: Doped garnets (llzo - type). Version 12. Citrination: https://citrination.com/datasets/184812/
28. Gastelum JCV, Strachan A (2019) Citrine tools for materials informatics. Retrieved from: https://nanohub.org/resources/citrinetools. https://doi.org/10.21981/EH1N-T337
29. Strachan A, Klimeck G, Lundstrom M (2010) Cyber-enabled simulations in nanoscale science and engineering. Comput Sci Eng 12(2):12–17
30. Wolfenstine J, Allen JL, Read J, Sakamoto J, Gonalez-Doncel G (2010) Hot-pressed $Li_{0.33}La_{0.57}Tio_3$. J Power Sources 195(13):4124–4128
31. Wolfenstine J, Rangasamy E, Allen JL, Sakamoto J (2012) High conductivity of dense tetragonal $Li_7La_3Zr_2O_{12}$. J Power Sources 208:193–196
32. Jha A, Chandrasekaran A, Kim C, Ramprasad R (2019) Impact of dataset uncertainties on machine learning model predictions: the example of polymer glass transition temperatures. Model Simul Mater Sci Eng 27(2):024002
33. Zeier WG (2014) Structural limitations for optimizing garnet-type solid electrolytes: a perspective. Dalton Trans 43(43):16133–16138
34. Thompson T, Sharafi A, Johannes MD, Huq A, Allen JL, Wolfenstine J, Sakamoto J (2015) A tale of two sites: on defining the carrier concentration in garnet-based ionic conductors for advanced li batteries. Adv Energy Mater 5(11):1500096
35. Pilania G, Wang C, Jiang X, Rajasekaran S, Ramprasad R (2013) Accelerating materials property predictions using machine learning. Sci Rep 3(1):1–6
36. Meredig B, Agrawal A, Kirklin S, Saal JE, Doak JW, Thompson A, Zhang K, Choudhary A, Wolverton C (2014) Combinatorial screening for new materials in unconstrained composition space with machine learning. Phys Rev B 89(9):094104
37. Ghiringhelli LM, Vybiral J, Levchenko SV, Draxl C, Scheffler M (2015) Big data of materials science: critical role of the descriptor. Phys Rev Lett 114(10):105503
38. Guyon I, Elisseeff A (2003) An introduction to variable and feature selection. J Mach Learn Res 3(Mar):1157–1182
39. Ward L, Agrawal A, Choudhary A, Wolverton C (2016) A general-purpose machine learning framework for predicting properties of inorganic materials. NPJ Comput Mater 2:16028
40. Cubuk ED, Sendek AD, Reed EJ (2019) Screening billions of candidates for solid lithium-ion conductors: a transfer learning approach for small data. J Chem Phys 150(21):214701
41. Jha D, Ward L, Paul A, Liao W, Choudhary A, Wolverton C, Agrawal A (2018) Elemnet: Deep learning the chemistry of materials from only elemental composition. Sci Rep 8(1):1–13
42. Butler KT, Davies DW, Cartwright H, Isayev O, Walsh A (2018) Machine learning for molecular and materials science. Nature 559(7715):547–555
43. Feng S, Zhou H, Dong H (2019) Using deep neural network with small dataset to predict material defects. Mater Des 162:300–310
44. Wager S, Hastie T, Efron B (2014) Confidence intervals for random forests: the jackknife and the infinitesimal jackknife. J Mach Learn Res 15(1):1625–1651
45. Hutchinson M (2016) Citrine informatics: Lolo. Retrieved from: https://github.com/CitrineInformatics/lolo
46. Kingma DP, Ba J (2014) Adam: a method for stochastic optimization. arXiv preprint arXiv:1412.6980
47. Caruana R, Lawrence S, Giles CL (2001) Overfitting in neural nets: backpropagation, conjugate gradient, and early stopping. In: Advances in neural information processing systems, pp 402–408
48. Chollet F et al (2015) Keras. Retrieved from: https://keras.io
49. Yang H, Zhang Z, Zhang J, Zeng XC (2018) Machine learning and artificial neural network prediction of interfacial thermal resistance between graphene and hexagonal boron nitride. Nanoscale 10(40):19092–19099
50. Wagner R, Rettenwander D, Redhammer GJ, Tippelt G, Sabathi G, Musso ME, Stanje B, Wilkening M, Suard E, Amthauer G (2016) Synthesis, crystal structure, and stability of cubic $Li_{7-x}La_3Zr_{2-x}Bi_xO_{12}$. Inorg Chem 55(23):12211–12219
51. Xue D, Balachandran PV, Hogden J, Theiler J, Xue D, Lookman T (2016) Accelerated search for materials with targeted properties by adaptive design. Nat Commun 7(1):1–9
52. Balachandran PV, Xue D, Theiler J, Hogden J, Lookman T (2016) Adaptive strategies for materials design using uncertainties. Sci Rep 6(1):1–9